SLOVAK UNIVERSITY OF
TECHNOLOGY IN BRATISLAVA
FACULTY OF ELECTRICAL ENGINEERING
AND INFORMATION TECHNOLOGY

Ing. Michal Sobota

Dissertation Thesis summary

DEVELOPMENT OF TECHNOLOGY FOR ORGANIC SENSORS WITH MOLECULAR SELECTIVITY

to obtain the Academic Title of Philisophiae doctor (PhD.)

in the study programme: Electronics and Photonics
in the study field: Electrical and Electronics Engineering

Place and Date: Bratislave, August 2024

Dissertation Thesis has been prepared at the Institute of Electronics and Photonics, Faculty of Electrical Engineering and Information Technology, Slovak University of Technology in Bratislava.

Submitter: Ing. Michal Sobota
Institute of Electronics and Photonics
Faculty of Electrical Engineering and Information Technology
Slovak University of Technology in Bratislava
Ilkovičova 3, 81219 Bratislava

Supervisor: Prof. Ing. Martin Weis, DrSc.

Opponents: prof. RNDr. Tibor Hianik, DrSc.
Univerzita Komenského v Bratislave
Fakulta matematiky, fyziky a informatiky
Katedra jadrovej fyziky a biofyziky

doc. RNDr. Pavol Vitovič, PhD.
Univerzita Komenského v Bratislave
Lekárska fakulta
Ústav medicínskeho vzdelávania a simulácií

Dissertation Thesis Abstract was sent: .....

Dissertation Thesis Defense will be held on ..... at .....
at Faculty of Electrical Engineering and Information Technology, Slovak University of Technology in Bratislava, Ilkovičova 3, 81219 Bratislava.

_____

Prof. Ing. Viera Stopjaková, PhD.
Chair of programme commision
of the study field Electrical and Electronics Engineering

Table of content

1 Introduction

Organic electronics is a well-established market player, mainly through organic light-emitting diode (OLED) and active-matrix organic light-emitting diode (AMOLED) devices; however, other possibilities are less well known. Solar cells are on the verge of vast commercialization. Still, the opportunity to exploit them lies in the organic field-effect transistor (OFET) based biosensor, the organic charge-modulated field-effect transistor (OCMFET). Only limited papers have been published; therefore, we tried to enrich the current knowledge. OCMFET offers superior stability among other organic-based biosensing structures.

At this moment, we incorporated OCMFET within the reversible light-stimulated metal-cation complexation on the OCMFET sensing area. Metal cations create a complex with isatin diarylhydrazone molecules prepared as a self-assembled monolayer (SAM), inducing charge in OCMFET and allowing quantitative analysis. Previous works by our cooperative team from the Faculty of Natural Sciences, Comenius University in Slovakia, led by Mr. Tisovský, included the complexation of free molecules in solution, which we enriched by the OCMFET sensing measurement [1, 2]. In Tab. 1, we summarize the World Health Organization (WHO) and similar European Union (EU) norms for transition metal concentrations in water [3, 4].

One of the already explored OCMFET applications is DNA biosensor, in our case, colorectal cancer (CRC) biomarker detection. This part of the work was done in cooperation with Mrs Veronika Šubjaková from the Faculty of Mathematics, Physics and Informatics, Comenius University Bratislava. The third most common cancer worldwide and the second most deadly cancer, killed only in 2020 almost 1 million people. These alarming

statistics are already high in countries of Western civilization and are increasing in semi-developed countries [5].

As a specific organic electronic category, organic electronics biosensors pose a chance for further development. Compared with inorganic analogies, it requires a lower fabrication effort with lower financial costs. The influential aspect is reliability conservation throughout the lifespan. Organic electronics can meet the drawbacks of inorganic biosensors, such as time-consuming measurements and relatively high expenses [6, 7].

Kergoat et al. (2012) [8] review OFET-based biosensors, including organic electrochemical transistors (OECTs), OFET operating in the dry state, OFET operating in the aqueous medium, ion-sensitive OFET (ISFET) and electrolyte-gated OFEET (EGOFET). These OFET-based architectures directly amplify the detected signal in the sensing device. The first organic charge-modulated field-effect transistor (OCMFET) fabricated by Demelas et al. (2012) [9] exposed the convenience of a floating gate where no reference electrode is needed. Also, the sensitivity of the OCMFET is theoretically independent of the usage of organic semiconductors [10]. Only a few studies have been published [9, 11–18], but there is a tremendous opportunity for impact for both research and commercial applications.

Crucial parts of OCMFET incorporate the organic semiconductor, the dielectric layer, contacts, the floating gate, the control gate, the active layer, and the encapsulation layer. Each of these parts of the device must be optimized to deliver high-efficiency measurement results.

Despite the preliminary results of OCMFET, further research is needed to prove the efficiency and rentability of OCMFET-based sensory systems, including OCMFET, device measurements, and data management systems.

A possible application method for organic biosensors could be publicly accessible preventive examinations, which may forego the

examination of the inorganic sensor in the case of the not-optimized technology of the organic biosensor. Overall, point-of-care and patient-oriented healthcare is the current trend.

2 Goals of the thesis

1) Design and fabricate organic field-effect transistor (OFET) devices, organic electrochemical transistor (OECT) devices, and organic charge-modulated field-effect (OCM-FET) devices with extended gate electrodes. Evaluate important electrical parameters of devices according to standards (IEEE 1620-2004) and compare them with already reported devices.

2) Verify device functionality with the receptor molecules. Select the proper receptor molecules as well as device design for pH evaluation, transition metal detection, or DNA detection in cooperation with Comenius University Bratislava.

3) Analyze the possibility of a patterned floating gate using atomic layer deposition (ALD) for gate insulator layers. Optimize the dielectric layer technology.

3 Brief state-of-the-art for an organic charge-modulated field-effect transistor (OCMFET)

The essential element for most electronics is silicon. It is a high-quality semiconductor that has decades of research behind it. As a result, it achieves high intrinsic mobilities, namely approximately 10^3 cm^2/Vs for electrons and 10^2 cm^2/Vs for holes at room temperature (300 K). Of course, these values change after doping. However, other semiconductors with similar or higher mobility are encountered in electronics [19–21].

Organic electronic is considered less expensive yet offer sufficient mobilities and overall performance. Various biosensing structures perspectives for economic biosensing, which could prevent diseases, have been proposed: organic electrochemical transistor (OECT), standard organic field-effect transistor (OFET) operating in dry state, electrolyte-gated OFET (EGOFET), ion-sensitive OFET (ISFET), and organic charge-modulated field-effect transistor (OCMFET).

Nowadays, the main goals for OECTs are increasing the active layer conductivity, increasing volumetric capacitance, increasing saturation mobility, and improving stability. Due to our biosensing aim, we mainly described methods for OECT stabilization, which also increase current performance. Most of the research is devoted to PEDOT: PSS as a standard active layer for OECT.

To date, OCMFET devices have been employed mainly for pH, DNA, pressure, and temperature sensors.

4 Main experimental methods

Atomic force microscopy (AFM) belongs to the category of scanning probe microscopy (SPM), which studies the surface morphology of materials. The prominent representatives of SPM are AFM and scanning tunnelling microscope (STM). The AFM is one of the essential apparatuses for analyzing sample morphology due to its excellent vertical resolution of ~0.1 nm.

Cyclic voltammetry (CV) is an electrochemical technique used to study chemical compounds' redox properties. It provides insights into reaction mechanisms, electron transfer kinetics, and the stability of intermediates. Electrochemical cells consist of three electrodes: working electrode (WE), reference electrode (RE), and counter electrode (CE). The solution where these electrodes are immersed standardly contains the analyte of interest and a supporting electrolyte to ensure conductivity.

Electrochemical impedance spectroscopy (EIS) provides detailed kinetic and mechanistic insights into various electrochemical systems. It is extensively utilized in fields such as corrosion studies, semiconductor science, energy conversion and storage technologies, chemical sensing, biosensing, and noninvasive diagnostics.

The **surface energy** of the dielectric layer significantly influences the growth of the organic semiconductor layer in OFET structures. Moreover, it can indicate surface functional groups. Generally, OSC materials form higher-quality layers with better-defined interfaces on dielectrics with lower surface energy.

5 Main experimental results

In the experimental part, we developed devices appropriate for biosensing applications. From the OECT technology, we were not able to sustain stability. Thus, we developed OCMFET technology with standard pH, novel transition metal and DNA CRC biomarkers.

The choice of the proper biosensing structure is a peculiar process. As seen in Fig. 1, we first tested OECT as very sensitive, but on the other hand, it was not stable enough. Afterwards, we focused on the OCMFET yielding stability and sacrificing adequate sensitivity. ISFET was not explored primarily due to problematic dielectric layer deposition on OSC, which is sensitive to high temperatures. EGOFET was not primarily explored because of direct contact of OSC with the electrolyte, which can dramatically affect stability, as was similarly seen for OECT.

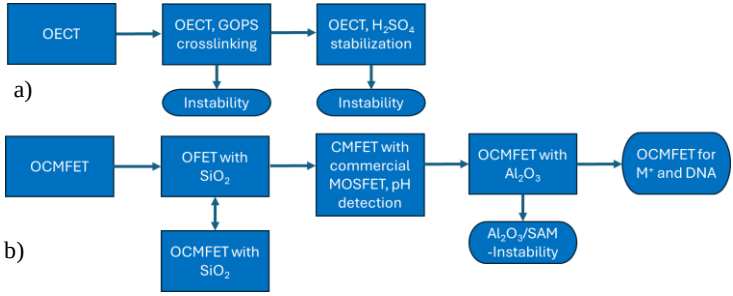

Fig. 1: Flowchart of organic transistor development for biosensing detection consisting of device structures a) OECT and b) OCMFET.

5.1 Organic electrochemical transistor

5.1.1 Evaporated electrodes, with printed cross-linked PEDOT: PSS, comparison of gate electrodes

We measured OECT with a commercially available Ag/AgCl electrode (Fig. 2 a – c). Subsequently, we measured the transistor with an identical series preparation, using an Ag/AgCl electrode prepared by electrolysis in a

saturated KCl solution (Fig. 2 d – f). The above waveforms show a comparable energy barrier between the two gate electrodes as expected; however, the stability of the Ag/AgCl electrode prepared by electrolysis is lower as the I_{ds} are reduced (Fig. 2 f).

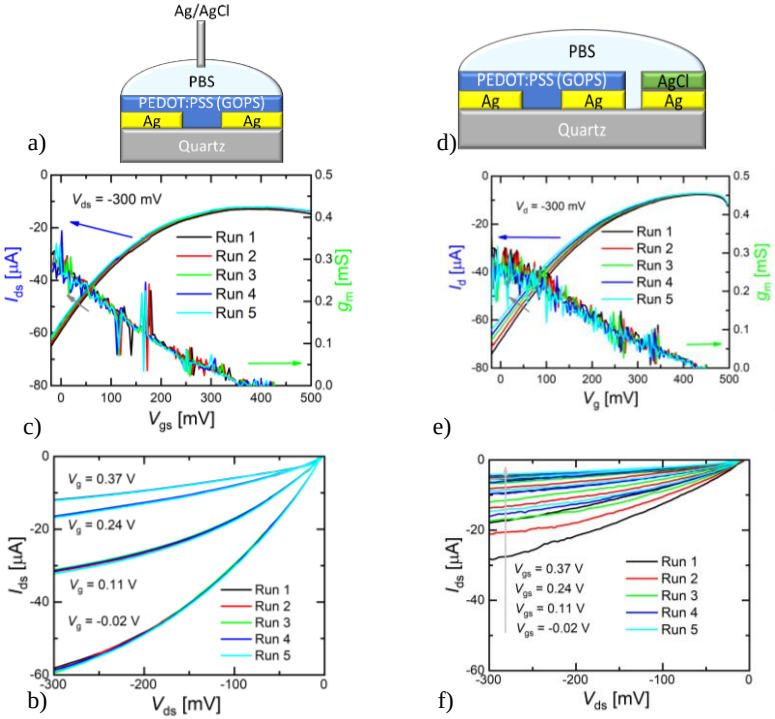

Fig. 2: a) Structure of OECT structure measured by the commercial Ag/AgCl electrode with b) transfer and c) output characteristics and d) structure measured by the Ag/AgCl electrode prepared by electrolysis along with the associated e) transfer and f) output characteristics.

According to Eq. 6.1, we obtain the mobility of the charge carrier in the saturated region (μ_{sat}), the transimpedance (g_m), and also the figure of merit (FOM), which is given by the product of μ_{sat} and the volumetric

capacitance (C^*, volumetric capacitance). Parameters W, L, d, V_t, g_m, and V_{gs} express the channel width, channel length, active layer thickness, threshold voltage, transconductance, and gate-source voltage, respectively. A comparison of the parameters thus obtained can be seen in Tab. 1. All of the above parameters were slightly better for the commercially available electrode, but these are comparable results. According to the literature, g_m and C* were similar to other results [22].

$$g_m = \frac{Wd}{L}\mu_{sat}C^*(V_t - V_{gs}) \tag{5.1}$$

Tab. 1: Comparison of the electrical parameters of the OECT measured by an Ag/AgCl electrode prepared by electrolysis with a commercially available electrode.

Ag/AgCl preparation method	g_m [mS]	μ_{sat} [cm^2/Vs]	$\mu_{sat}C^*$ [F/cmVs]
Electrolysis	0.24	6.3×10^{-3}	3.3×10^{-2}
Commercial	0.28	6.8×10^{-3}	3.5×10^{-2}

Due to the better stability of the commercial Ag/AgCl electrode, we measured the stability of the transistors in the switched-on state only for the OECT prepared in this way (Fig. 3); however, I_{ds} showed a time instability reaching ~10 % deviation from the initial current in 15 min.

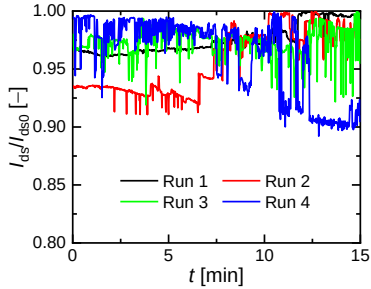

Fig. 3: The drain-source current of the OECT in the switched-on state during four 15-minute measurements with a commercial Ag/AgCl electrode (V_{gs} = -20 mV, V_{ds} = -300 mV).

5.1.2 Fully printed organic electrochemical transistor (flexible substrate), EIS acquisition

We successfully fabricated the OECT using inkjet printing only, which allowed the use of a flexible substrate shown in the micrograph (Fig. 4 a). A schematic of the structure is shown in Fig. 4 b). Using electrochemical impedance spectroscopy (EIS) of the Ag/PEDOT: PSS/DI+PBS/AgCl/Ag structure, we were able to obtain C^* for PEDOT: PSS by fitting the measured data with an equivalent electric circuit inset of a Randles circuit (Fig. 4 c inset) equivalent electric circuit inset). R1 and R2 are the resistors, C1 is the capacitance of the electrical double layer between the electrolyte and PEDOT: PSS and W1 is the Warburg term describing the charge carriers' diffusion process.

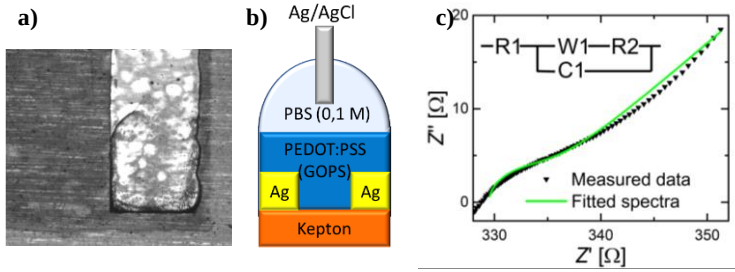

Fig. 4: a) Monochrome micrograph of an inkjet-printed silver electrode (right – light grey) with an overlayer of PEDOT: PSS (left – dark grey), b) Structure of the whole printed OECT and c) Nyquist plot of the EIS with the embedded electrical equivalent circuit. The measured frequencies ranged from 1 kHz to 1 MHz.

5.1.3 Fully printed organic electrochemical transistor, H_2SO_4 treatment

In the previous experiment, we used the same structure for inkjet printing, but due to the instability of PEDOT: PSS in the last experiment (Fig. 5), PEDOT: PSS was not cross-linked. However, we used the treatment of PEDOT: PSS in a concentrated 96 % H_2SO_4, which, according to the

literature, is beneficial for increasing stability and electrical conductivity. We also stayed for stability with the commercial Ag/AgCl electrode.

For better tracking of the change in electrical resistivity, we opted for real-time monitoring (Fig. 6). We monitored resistance before and during H_2SO_4 treatment, during rinse in DI, and at the end after nitrogen drying.

Also, Raman spectroscopy confirms the "fingerprint" for PEDOT: PSS, which was not disturbed even by measurement in the electrolyte.

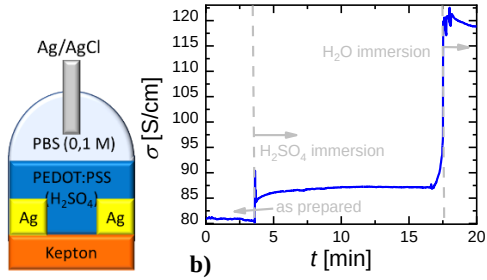

Fig. 6: a) Structure of OECT prepared with PEDOT: PSS (H_2SO_4), b) subsequent immersion in H_2SO_4 and DI.

For the EIS of the prepared PEDOT: PSS with treatment in H_2SO_4, we plotted the Nyquist plot with Randles circuit fitting in the inset electrical equivalent circuit in Fig. 8. Thus, we obtained C^*=53.87 F/cm^3.

While measuring the prepared and characterized OECT elements in this way, we measured the transfer and output characteristics multiple times (Figs. 7 a and b), from which we evaluated the electrical parameters in Tab. 2. As can be seen, μ_{sat} and FOM reached 1.5×10^{-5} cm^2/Vs and 7.8×10^{-4} F/cmVs, respectively. As can be seen from the stability measurements (Fig. 7 c), I_{ds} changed only ~2 % in 15 min. The increase in stability can be related to a lower μ_{sat}, which is not necessarily convenient, as can be seen in FOM $\mu_{sat}C^*$ reaching only 7.8×10^{-4} F/cmVs.

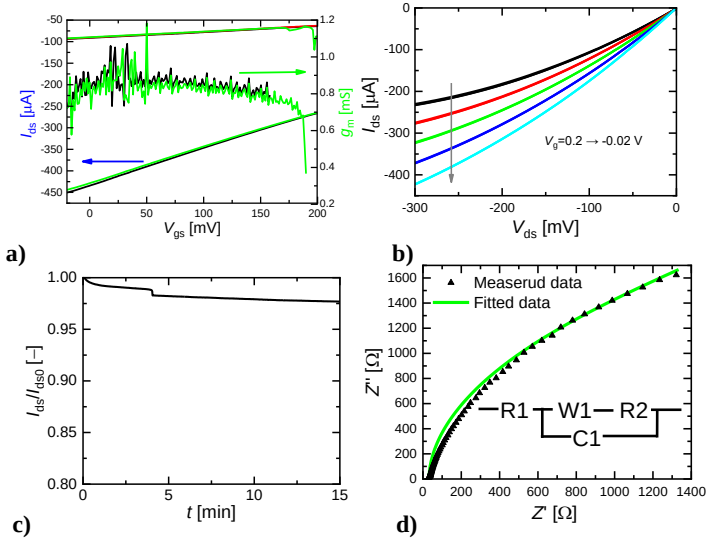

Fig. 7: Structure of the OECT measured by a commercial Ag/AgCl electrode with a) transfer and b) output characteristics and c) stability measurement of the stability of the OECT in the switched state (V_{gs} = -20 mV, V_{ds} = -300 mV), and d) Nyquist plot of the EIS with an embedded electrical equivalent circuit. The measured frequencies ranged from 1 Hz to 1 MHz.

Tab. 2: Comparison of the electrical parameters of fully-printed OECT measured by a commercial Ag/AgCl.

Ag/AgCl preparation methods	g_m [mS]	μ_{sat} [cm^2/Vs]	$\mu_{sat}C^*$ [F/cmVs]
Commercial	0.9	1.5×10^{-5}	7.8×10^{-4}

First, we stabilized PEDOT: PSS by GOPS cross-linking. The increased stability of OECT was not sufficient. Noisy I_{ds} changed as high as ~10 % in 15 min (Tab. 9). In Chapter 5.1.2, we achieve fully printed OECT, easing the preparation process and quantifying C^* by EIS. In Chapter 7.1.3, we approach stabilizing PEDOT: PSS by treatment with H_2SO_4 as another common approach, improving the change in I_{ds} by ~2 % at the expense of

lowering FOM. PEDOT: PSS stability issues are as limitedly published as a well-known fact [23–26].

Tab. 3: Comparison of the electrical parameters of the OECT measured by the commercial Ag / AgCl electrode from Chapters 5.1.1 and 5.1.3.

PEDOT: PSS preparation method	$\mu_{sat}C^*$ [F/cmVs]	I_{ds}/I_{ds0} in 15 min [-]
GOPS cross-linking	3.5×10^{-2}	~0.1
Treatment with H_2SO_4 treatment	7.8×10^{-4}	~0.02

5.2 Organic charge-modulated field-effect transistor

Due to the stability issues described in previous chapters, a new focus has been placed on the promising yet unrecognized area of OCMFETs.

5.2.1 Al_2O_3 optimization

Al_2O_3 growth was separately optimized to achieve suitable electrical parameters: relative permittivity (ε_r) and dielectric strength (E_{br}). The temperature was set at 300 °C as previously optimized [27]. The tested preparation techniques included O_3 and H_2O. Metal-insulator-metal (MIM) structures consisted of Au/Al_2O_3/Ag.

Atomic layer deposition (ALD) O_3 exposure reached superior properties (Tab. 4). As expected, the thinner oxides reached a lower E_{br} and a higher C_n and ε_r. Therefore, in further experiments, an O_3 atmosphere was used.

Tab. 4: Comparison of electrical quantities of Al_2O_3 ALD prepared by different exposures.

Preparation atmosphere	h [nm] (Ellipsometry)	C_n [nF/cm^2]	E_{br} [MV/cm]	ε_r [-]
O_3	14.01	601±7	6.5±0.4	9.5±0.1
	9.24	672±1	4.8	7.0±0.1
H_2O	15.4	504±6	1.4	8.8±0.1
	9.57	804	0.9	8.7

5.2.2 OCMFET with hybrid dielectric layer

From nonfunctionalized OCMFETs (Fig. 8 b), we acquired standard OFET characteristics (Fig. 8). μ_{sat} were the highest for the Al_2O_3 and OTS–modified surface, thus prerequisite them for OCMFET sensing measurements. Unfortunately, the OTS and ODPA OCMFETs struggled to be reproducible as theoretically described.

For the final OCMFET design, theoretical sensitivity was estimated according to Eq. 4.3, yielding 5.2×10^7 V/C with an Al_2O_3 capacitance of 0.003 F/m^2.

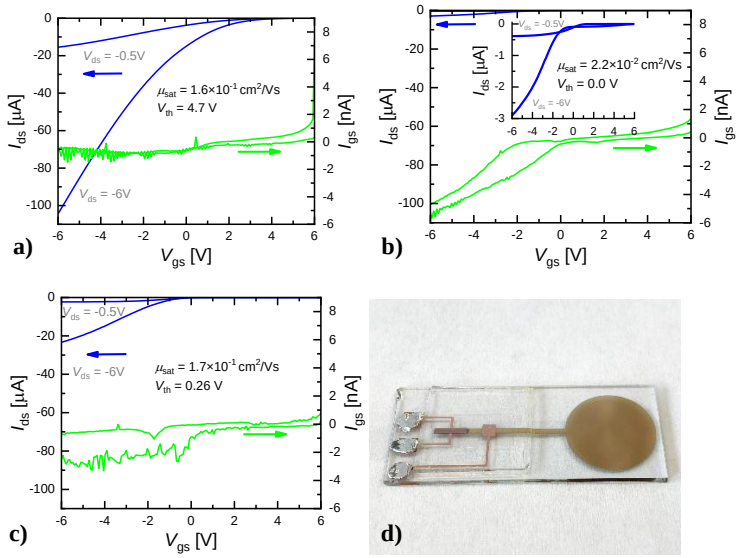

Fig. 8: OCMFET with a dielectric layer of a) Al_2O_3, b) Al_2O_3/ODPA, c) Al_2O_3/OTS, and d) actual sample with indium contacts.

5.2.3 pH detection

For the *pH* detection, the bare Au surface of the OCMFET floating gate was exposed to cysteamine hydrochloride water solution. From standard transfer OCMFET characteristics, we derived threshold voltage (V_{th}), which was

further evaluated. The quasi-logarithmic behaviour of V_{th} corresponds to filling the trap states during multiple measurements that are standardly seen for organic electronics, which manifests as V_{th} hysteresis [28]. We fitted V_{th} by an exponential function and subtracted it from our measurement (Fig. 9). Reached pH dependence was fitted by two empirical models biphasic dose response function (BiDoseResp, coefficient of determination - $R^2 = 0.80$) and five parameters logistic function (Logistic5, $R^2 = 0.93$), which is much simpler model reaching superior R^2. Another physically anchored Langmuir adsorption model describes dynamical adsorption and desorption ($R^2 = 0.90$) depending on pressure. pH measurements were consistent with EIS and CV measurements.

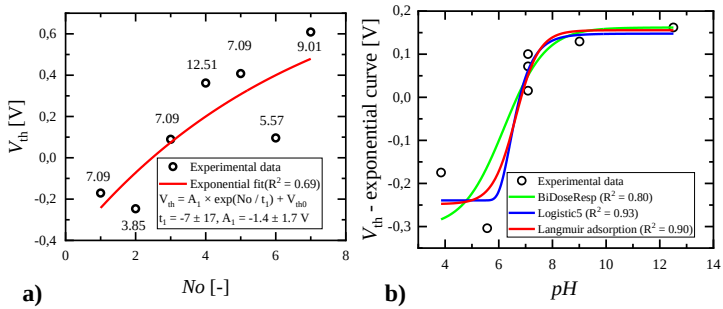

Fig. 9: a) pH sensing with V_{th} analysis and b) V_{th} calibration curve depiction subtracted exponential trend.

5.2.4 Transition metals detection

For the transition metal detection, the bare Au surface of the OCMFET floating gate was exposed to isatin diarylhydrazone complex (Fig. 10 a) consisting of binder and hydrazon SAMs in ethanol. OCMFET remained only partially immersed, leaving an encapsulated part above the ethanol.

From the switched-on state of OCMFET with the aforementioned active layer preparation, we measured static concentration of 10 mM $ZnCl_2$ in DI, testing reversibility of Zn^{2+} cation binding (Fig. 10). Another conducted

test in situ revealed standard I_{ds} decrease due to OSC trapping [29–31] called bias-temperature stress (BTS) established for inorganic a-Si TFTs. However, this exponential model was slightly altered with the second exponential component since one could not describe the I_{ds} well. We can only hypothesize different trap states charging or other charging with an unknown origin. We successfully present corrected I_{ds} with the calibration curve.

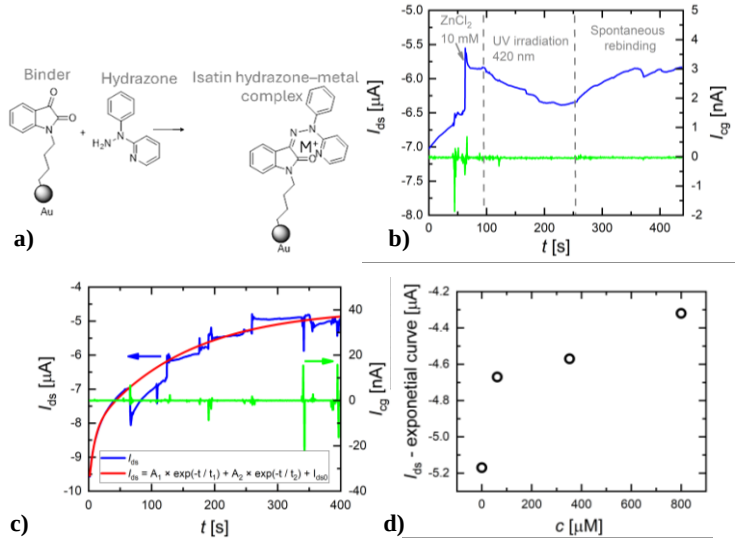

Fig. 10: a) SAM preparation of isatin hydrazone molecule from binder and hydrazone, b) OCMFET Zn^{2+} detection a) ON-state reversible photoswitchable detection, b) in-situ calibration for concentration, and d) calibration curve.

5.2.5 DNA detection

OCMFET remained partially immersed, leaving an encapsulated part above the DNA solution. Immobilization with thiol groups was chosen due to its size and high affinity of sulfur to gold. Compared to avidin-streptavidin, thiol group is not expected to pose a high charge inhibiting electric field to floating gate [32].

Three ssDNA sequences were commercially purchased as follows:

- 3'-AAA AAA AAA AAA AAA AAA AAA TGG ACT TTT TCC AAT-5' (Healthy)
- 3'-AAA AAA AAA AAA AAA AAA AAA AAA TGG ACT TTT TCC AAT-5' (Marker)
- Thiol-5'-(9×A)-TTT TTT TTT TTT TTT TTT TTT TTT ACC TGA AAA AGG TTA-3' (Sensory)

The thiol group served for immobilization on gold, and nine adenines in Sensory ssDNA served as spacer to allow correct hybridization of complementary ssDNA not to be 'overgrown' by mercaptohexanol (MCH). Three starting A in healthy ssDNA are not complementary to sensory AAA from sensory ssDNA, theoretically contradicting hybridization.

Electrochemical measurements consisted of standard Au electrochemical cleaning in H_2SO_4, sensory ssDNA immobilization on Au in overnight. Afterwards, 1 h of MCH took place filling the space between the ssDNA (Fig. 11). Finally, 1 μM ssDNA of Healthy or Marker ssDNA was incubated for 1 h which was monitored by EIS.

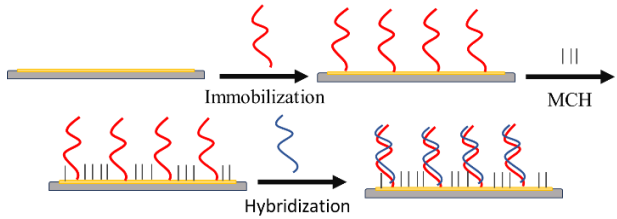

Figure 11: ssDNA immobilization, MCH, and DNA hybridization on the gold electrode.

EIS were taken after sensory subsequent incubation of ssDNA and MCH in potassium hexanocyanoferrate(III) ($K_3[Fe(CN)_6]$) solution (tag – immobilization in Fig. 12) and after hybridization (tag – hybridization). From the EIS of complementary ssDNA (Marker) to ssDNA (Sensory), only 2 out

of 5 samples (40 %) exhibited an increase in capacitance, which is attributed to the formation of dsDNA formation (tag – stable, Fig. 13). EIS were repeatedly measured to confirm reliability. The equivalent circuit was not evaluated due to low reproducibility. The decrease or absence of change in capacitance signify instability of DNA adhesion or wrong DNA orientation and/or stacking on Au possibly caused by erroneous incubation times or multiple spacer adenines in sensory ssDNA adsorption on Au (tag - instable) [32].

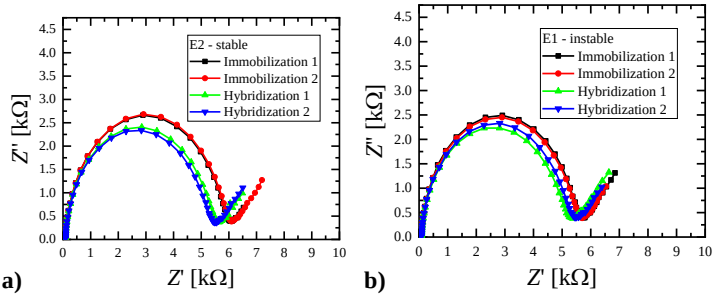

Figure 12: Examples of EIS monitoring of a) stable and b) instable complementary – marker hybridization DNA for various samples.

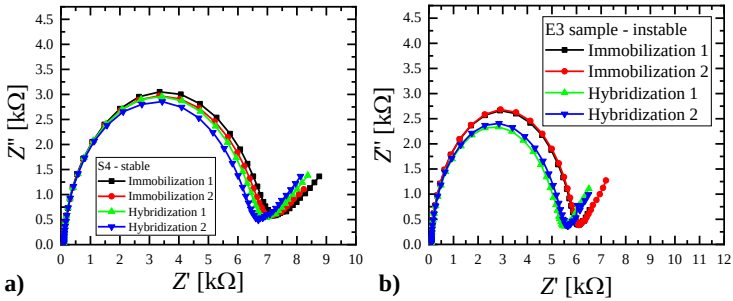

Figure 13: Examples of EIS a) stable and b) instable monitoring of non-complementary – marker DNA for various samples.

Furthermore, non-complementary ssDNA – Healthy exhibited two relative stability of no change (tag – stable) caused by no or negligible interaction of non-complementary ssDNA with sensory ssDNA (Fig. 14). The other two runs exhibited increases or decreases in capacitance, implying sensory DNA instability and interaction of non-complementary DNA (tag - instable). The resulting yield of the stable mechanism is thus 50 %.

Despite the relative instability of the EIS, we acquired a standard transfer curve of the OCMFET despite a certain weakness of the dielectric layer - I_{gs} compliance (Fig. 14). Hybridization was monitored in situ after 1, 2, and 3 hours. From the V_{th} analysis, we again acquired a higher certainty for V_{th2}. V_{th2} shift indicates DNA hybridization; however, due to the ambiguity of EIS, we cannot confirm the results.

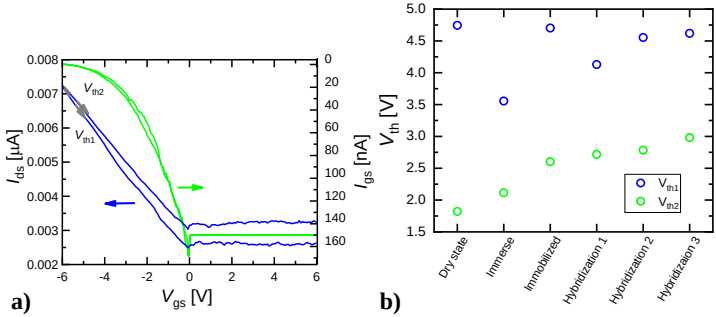

Figure 14: a) Standard OCMFET transfer characteristic and b) hybridization monitoring.

6 Summary of dissertation results

The main results achieved in this work can be written as follows:

- New insights into organic electronics-based biosensors have been gained.
- New knowledge was gained on the operation and parameter evaluation of organic field-effect transistors.
- Methods for the preparation and characterization of thin films in order to optimize their electrical parameters and film quality were introduced.
- Research activities were focused on debugging the technology necessary to produce high quality field-effect transistors.
- Optimized preparation conditions of organic electrochemical transistor in order to increase stability.
- Optimized shadow masks, gold adhesion layer, photolithography process as well as atomic layer deposition (ALD) parameters.
- The experiments performed proved the possibility of preparing field-effect transistors using ALD with self-assembled SAM layers.
- The pH measurements were modeled using two empirical and one newly-adapted Langmuir adsorption model.
- Innovative transition metal detection with photoreversibility and calibration curve using OCMFET device.
- Detection of colorectal cancer DNA biomarkers using OCMFET.

7 Conclusion

This work dealt with biosensor transducer development for practical application. OFET-based biosensors excel in built-in signal amplification.

From a literature review, we extracted possible OFET and OECT-based biosensing structures, and standard materials for usage. OECT and OCMFET were proposed as the most perspective option for precise biomolecule detection. High volumetric capacitance increases OECT perspectives for sensory application, on the other hand OCMFET offers lower sensitivity sacrificed for stability. Also, the literature review offered us insight into biomolecule recognition mechanism by the biorecognition molecules. Standard pH sensing, novel transition metal and CRC DNA biomarker were further analyzed.

During OECT development, two reference electrodes were compared: electrochemically deposited and commercial, which performed more stable. $\mu_{sat}C^*$ FOM of PEDOT: PSS (GOPS) OECT with commercial 3.5×10^{-2} F/cmVs. Despite that, the time characterization of the Ids of the switched-on device reached as high as ~10 % variation of ~10 % in 15 min. We were able to prepare fully printed OECTs with H_2SO_4 treatments for the stabilization and PEDOT: PSS conductivity enhancement, however, stability reached ~2 % sacrificing $\mu_{sat}C^*$. In situ conductivity was monitored corresponding with Raman spectra that revealed a decrease in PSS strain content.

In the technology verification experiment of OFET with a control gate was done. Typical IV characteristics exhibited mastered OFET technology. Important OFET parameters comparison of sole OFET and OFET with control gate have been evaluated, such as average μ_{sat} = 0.081±0.002 cm^2/Vs for sole OFET, μ_{sat} = 0.034±0.025 cm^2/Vs for OFET with control gate, V_{th}, and I_{ds_Max}. In the second experiment run, improved OFET parameters offered

a deeper investigation possibility. Mobilities as high as 0.39 cm^2/Vs for sole OFET and 0.12 cm^2/Vs for the OFET with control gate exhibited comparable results from a literature review. High V_{th} = 26.4 V of OFET with control gate needs to be corrected. SS = 5.1 V/dec and $N_{\square} = 12.5\times10^{12}\ cm^{-2}$ for OFET with control gate performed as expected lower than SS = 2.8 V/dec and $N_{\square} = 2.8\times10^{12}\ cm^{-2}$. We attribute higher $I_{on/off}$ for OFET measurement to the low V_{th}.

During OCMFET optimization, the process switched from interdigit to single channel OCMFET design, due to higher process yield i.e. shadow mask alignment improvement. We also inspected golds surface roughness on SiO_2 with MPTMS and Ni adhesion layers. Despite optimized roughness of SiO_2/Ni/Au structure (S_q=1.38), delamination during Al_2O_3 etching due to high surface tension of water forced us to slightly more standard adhesion layer of Cr, which has convenience over Ti by possibility of thermal evaporation compared to ion-beam sputtering.

Al_2O_3 ALD process was optimized in terms of electrical parameters. O_3 reached higher E_{br} (6.5±0.4) and C_n (601±7 nF/cm^2) compared to the H_2O atmosphere. ε_r reached 9.5±0.1 for 14.01 nm dielectric layer. Due to negative photoresist requirement of ultrasound during stripping, we exhibited structural defect as was examined on separate MIM structures. Thus, we changed the photolithography process on positive photoresist without ultrasound need. In the meantime of photolithography development, we discovered superior adhesion of Cr, therefore, we got rid of photolithography process, enabling us speed up the process. Minor effort was also done on evaporation technique resolution limits. It was found out that masks nominal circle area 0.1 mm^2 during evaporation reached 0.0951 mm^2, reaching coefficient of variation 4.7 %. Therefore, circle areas larger and equal to nominal area 0 .1 mm^2 reached area error below 5 %. Overspray of

evaporation structures was also manifested during ε_r estimation, which was dependable on area size mainly significant for smaller areas.

From previously optimized OCMFET technology, we prepared three OCMFETs differing dielectric layer: bare Al_2O_3, Al_2O_3/OTS, Al_2O_3/ODPA, reaching best performance for bare Al_2O_3 (μ_{sat} = 1.6 × 10^{-2} cm^2/Vs, V_{th} = 4.7 V). Unfortunately, these pilot dielectric hybrid layers emerged problematic, because of stability during further technological steps.

During pH sensing by OCMWET we examined hysteresis analysis by subtraction of exponential charging background. V_{th} vs. pH dependance was modeled by two empirical models of BiDoseResp (R^2 = 0.80) and Logistic5 (R^2 = 0.93). Finaly, a new model for pH OCMFET, Langmuir adsorption (R^2 = 0.90) was analyzed, which is physically anchored. pH sensing was further confirmed by EIS and CV.

Novel metal ion detection was performed by hydrazine-based molecule, which exhibited photoreversibility, and calibration curve with four points. Previously, only solution sensing by absorption spectroscopy was reported.

Finaly, BAT26 biomarker sensory ssDNA was designed for OCMFET purposes. V_{th2} shift indicated DNA hybridization, however from ambiguity of EIS, we cannot confirm the biorecognition of DNA.

Organic electronic biosensors pose an extraordinary field of perspective research for practical application, enriching the current organic electronics application range. Challenges in the OFET-based biosensors encompass sufficiently high stability and reproducibility are worth of relatively low costs and lower ecological footprint.

8 Schlussfolgerung

Diese Arbeit widmet sich der Entwicklung von Biosensor-Wandlern für die praktische Anwendung. OFET-basierte Biosensoren zeichnen sich durch eine integrierte Signalverstärkung aus.

Anhand einer Literaturrecherche haben wir mögliche OFET- und OECT-basierte Biosensorstrukturen und Standardmaterialien für die Verwendung ermittelt. OECT und OCMFET wurden als die aussichtsreichste Option für den präzisen Nachweis von Biomolekülen vorgeschlagen. Die hohe volumetrische Kapazität erhöht die Aussichten von OECT für sensorische Anwendungen, während OCMFET eine geringere Empfindlichkeit zu Lasten der Stabilität bietet. Dank der Literaturrecherche haben wir auch einen Einblick in den Erkennungsmechanismus von Biomolekülen durch die Biorecognition-Moleküle bekommen. Für weitere Analysen waren Standard-pH-Sensoren, neuartige Übergangsmetalle und CRC-DNA-Biomarker ausgewählt.

Während der OECT-Entwicklung wurden zwei Referenzelektroden verglichen: eine elektrochemisch abgeschiedene und eine kommerzielle, die sich als stabiler erwies. $\mu_{sat}C^*$ FOM von PEDOT: PSS (GOPS) OECT mit kommerziellen $3{,}5\times10^{-2}$ F/cmVs. Trotzdem erreichte die zeitliche Abhängigkeit der Ids des eingeschalteten Bauelements eine Variation von ~10 % in 15 Minuten. Wir waren in der Lage, vollständig gedruckte OECTs mit H_2SO_4-Behandlungen zur Stabilisierung und PEDOT: PSS-Leitfähigkeitsverbesserung herstellen, jedoch erreichte die Stabilität nur ~2 %, was zu Verlust von $\mu_{sat}C^*$ fuhr. Die In-situ-Leitfähigkeit wurde anhand von Raman-Spektren überwacht, die eine Abnahme des PSS-Dehnungsgehalts zeigten.

Im Rahmen der Technologieverifizierung wurde ein Experiment mit einem OFET mit Kontrollgate durchgeführt. Standarde IV-Eigenschaften

zeigten, dass die OFET-Technologie erfolgreich beherrscht war. Es wurden wichtige OFET-Parameter zwischen dem OFET und dem OFET mit Steuergate verglichen, wie z.B. μ_{sat} = 0,081±0,002 cm^2/Vs für den OFET, μ_{sat} = 0,034±0,025 cm^2/Vs für den OFET mit Steuergate, V_{th} und I_{ds_Max}. Im zweiten Experimentdurchlauf boten verbesserte OFET-Parameter eine tiefere Untersuchungsmöglichkeit. Mobilitäten von bis zu 0,39 cm^2/Vs für den OFET und 0,12 cm^2/Vs für den OFET mit Kontrollgate zeigten vergleichbare Ergebnisse wie in der Literatur. Die hohe V_{th} = 26,4 V des OFET mit Kontrollgates musste korrigiert werden. SS = 5,1 V/dec und $N_{\square}$ = 12,5×10^{12} cm^{-2} für den OFET mit Kontrollgates schnitten erwartungsgemäß schlechter ab als SS = 2,8 V/dec und $N_{\square}$ = 2,8×10^{12} cm^{-2}.

Während der OCMFET-Optimierung wurde der Prozess von einem Interdigit- auf ein Einkanal-OCMFET-Design umgestellt, um die Prozessausbeute zu erhöhen, d. h. die Anlehnung der Schattenmaske zu verbessern. Wir untersuchten auch die Oberflächenrauheit von Gold auf SiO_2 mit MPTMS- und Ni-Haftschichten. Trotz der optimierten Rauheit der SiO_2/Ni/Au-Struktur (S_q = 1,38) zwang uns die Delaminierung während des Ätzens von Al_2O_3 aufgrund der hohen Oberflächenspannung von Wasser dazu, eine etwas standardmäßigere Haftschicht aus Cr zu verwenden.

Der Al_2O_3 ALD-Prozess wurde hinsichtlich der elektrischen Eigenschaften optimiert. O_3 erreichte höhere E_{br} (6,5±0,4) und C_n (601±7 nF/cm^2) im Vergleich zur H_2O-Atmosphäre. ε_r erreichte 9,5±0,1 für 14,01 nm dielektrische Schicht. Aufgrund des negativen Photoresist-Bedarfs von Ultraschall während des Strippens zeigten sich strukturelle Defekte, wie sie an separaten MIM-Strukturen untersucht wurden. Daher änderten wir den Fotolithografieprozess auf positiven Photoresist ohne Ultraschallbedarf. Während der Entwicklung der Fotolithografie entdeckten wir eine bessere Haftung von Cr, so dass wir den Fotolithografieprozess abschafften und den Prozess beschleunigen konnten. Geringe Anstrengungen wurden auch bei den

Auflösungsgrenzen der Verdampfungstechnik unternommen. Es wurde festgestellt, dass die nominale Kreisfläche der Maske von 0,1 mm2 während des Aufdampfens 0,0951 mm^2 erreichte, was einem Variationskoeffizienten von 4,7 % entspricht. Daher erreichten Kreisflächen, die größer und gleich der Nennfläche 0,1 mm^2 waren, einen Flächenfehler von unter 5 %. Das Übersprühen von Verdampfungsstrukturen zeigte sich auch bei der ε_r Schätzung, die von der Flächengröße abhing, und vor allem bei kleineren Flächen signifikant war.

Ausgehend von der zuvor optimierten OCMFET-Technologie haben wir drei OCMFETs mit unterschiedlichen dielektrischen Schichten hergestellt: nacktes Al_2O_3, Al_2O_3/OTS, Al_2O_3/ODPA, wobei die beste Leistung für nacktes Al_2O_3 erreicht wurde (μ_{sat} = 1,6 × 10^{-2} cm^2/Vs, V_{th} = 4,7 V). Leider erwiesen sich diese dielektrischen Pilot-Hybridschichten als problematisch in Bezug auf die Stabilität während weiterer technologischer Schritte.

Bei der pH-Messung durch OCMFET haben wir die Hystereseanalyse durch Subtraktion des exponentiellen Ladungshintergrunds untersucht. Die Abhängigkeit der Vth vom pH-Wert wurde mit zwei empirischen Modellen modelliert: BiDoseResp (R^2 = 0,80) und Logistic5 (R^2 = 0,93). Schließlich wurde ein neues Modell für pH OCMFET, die Langmuir-Adsorption (R^2 = 0,90), analysiert, das physikalisch verankert ist. Die pH-Erkennung wurde durch EIS und CV bestätigt.

Die neuartige Metallionendetektion wurde mit einem Molekül auf Hydrazinbasis durchgeführt, das eine Photoreversibilität und eine Kalibrierungskurve aufwies. Zuvor wurde nur über die Erkennung von Lösungen durch Absorptionsspektroskopie berichtet.

Schließlich wurde für OCMFET-Zwecke ein BAT26-Biomarker-Sensor für ssDNA entwickelt. Die V_{th2}-Verschiebung deutet auf eine DNA-

Hybridisierung hin, aber aufgrund der Mehrdeutigkeit der EIS können wir die biologische Erkennung der DNA nicht bestätigen.

Organisch-elektronische Biosensoren stellen ein außerordentliches Forschungsfeld für die praktische Anwendung dar. Diese Dissertationsarbeit erweitert den derzeitigen Anwendungsbereich der organischen Elektronik. Trotz der Stabilitäts- und Reproduzierbarkeitsprobleme bei den OFET-basierten Biosensoren sind wir der Meinung, dass diese aufgrund ihrer relativ geringen Kosten und eines geringeren ökologischen Fußabdrucks weitere Forschung wert sind.

9 Publikačná činnosť

V3 Vedecké práce v zahraničných karentovaných časopisoch (4)

[1] **SOBOTA, Michal**; AHMADI, Soha; LOTAY, Navina; THOMPSON, Michael; WEIS, Martin. Exploring Electrochemically Prepared Carbon Dots Post-treatments with Amphiphilic and Nonamphiphilic Surfactants. New Journal of Chemistry, Accepted Manuscript 11.7.2024, First published 25.7.2024 (DOI: https://doi.org/10.1039/D4NJ01073F)

[2] FERIANCOVÁ, Lucia [45%]; CIGÁŇ, Marek [5%]; KOŽÍŠEK, Jozef [5%], GMUNCOVÁ, Katarína [5%], NÁDAŽDY, Vojtech [5%]; DUBJA, Tibor [5%]; **SOBOTA, Michal** [5%]; NOVOTA, Miroslav [5%]; WEIS Martin [5%]. Dithienylnaphthalenes and quaterthiophenes substituted with electron-withdrawing groups as n-type organic semiconductors for organic field-effect transistors. Journal of Materials Chemistry C, 10, s. 10058-10074.
Uložené v databáze: SCOPUS: 2-s2.0-85133775053

[3] EGYENES, Fridrich [16%]; GUCMAN, Filip [12%]; HUŠEKOVÁ, Kristína [12%]; DOBROČKA, Eduard [12%]; **SOBOTA, Michal** [12%], MIKOLÁŠEK, Miroslav [12%]; FRÖHLICH, Karol [12%]; ŤAPAJNA, Milan [12%]. Growth of alpha- and beta-Ga(2)O(3)epitaxial layers on sapphire substrates using liquid-injection MOCVD. Semiconductor Science and Technology, 35, s. 115002
Uložené v databáze: SCOPUS: 2-s2.0-85092570422

[4] KOSNÁČOVÁ, Helena [27%]; HORVÁTH, Dušan [10%]; STRÉMY, Maximilán [6%]; **SOBOTA, Michal** [4%]; BARTOŠ, Patrik [7%]; JAGELKA, Martin [4%]; ZÁVODNÍK, Tomáš [4%]; VIŤAZKOVÁ, Diana [5%]; FOLTÁN, Erik [3%]; VRČEK, Neven [3%]; VAVRINSKÝ, Erik [27%]. Pilot experiments and hardware design of smart electrooculographic headband for people with muscular paralysis. IEEE Access, 12, s. 49106-49121
Uložené v databáze: SCOPUS: 2-s2.0-85188439398

V2 Publikované príspevky na domácich vedeckých konferenciách (13)

[1] **SOBOTA, Michal** [17%]; NOVOTA, Miroslav [17%]; FERIANCOVÁ, Lucia [17%]; PUTALA, Martin [17%];

GMUNCOVÁ, Katarína [16%]; WEIS, Martin [16%]. Electrical characterization of new high mobility N-type semiconductors based on quatertiophene. ADEPT 2021. Žilina: Vydavateľstvo EDIS, 2021, s. 151-154. ISBN 978-80-554-1806-3.

[2] VARĎŽÁK, Adam [5%]; **SOBOTA, Michal** [5%]; NOVOTA, Miroslav [30%]; MIČJAN, Michal [30%]; WEIS, Martin [30%]. Encapsulation of organic electronics devices. 21. Škola vákuovej techniky. Bratislava: Slovenská vákuová spoločnosť, 2019, s. 154-157. ISBN 978-80-99905-01-7.

[3] MIČJAN, Michal [60%]; KOHLMANN, Lukáš [5%]; **SOBOTA, Michal** [10%]; NOVOTA, Miroslav [20%]; WEIS, Martin [5%]. Evaluation of Contact Resistance in Dntt Organic Field-Effect Transistors with Copper Top Electrodes. ADEPT 2023. Žilina: Vydavateľstvo EDIS, 2023, s. 189-192. ISBN 978-80-554-1977-0.

[4] MIČJAN, Michal [35%]; KOHLMAN, Lukáš [5%]; **SOBOTA, Michal** [20%]; NOVOTA, Miroslav [20%]; WEIS, Martin [20%]. Evaluation of organic semiconductor parameters of dntt in organic field-effect transistor devices. ADEPT 2022. Žilina: Vydavateľstvo EDIS, 2022, s. 234-237. ISBN 978-80-554-1884-1.

[5] **SOBOTA, Michal** [30%]; KOLENČÍK, Filip [5%]; STUCHLÍKOVÁ, Ľubica [35%]; WEIS, Martin [30%]. Importance and implementation of virtual reality for organic photovoltaic educational purposes. ICETA 2023. Danvers: Vydavateľstvo IEEE, 2023, s. 479-484. ISBN 979-8-3503-7068-3.

[6] **SOBOTA, Michal** [80%]; MIČJAN, Michal [10%]; WEIS, Martin [10%]. Monitoring the conductivity improvement of PEDOT:PSS using sulfuric acid in real time. Fotonika 2022. Bratislava: Vydavateľstvo: Medzinárodné laserové centrum, 2022, s. 93-96.

[7] **SOBOTA, Michal** [40%]; KOKAVEC, Ondrej [5%]; MIČJAN, Michal [10%]; NOVOTA, Miroslav [10%]; WEIS, Martin [35%]. Organic electrochemical transistors for biosensing applications. ASDAM 2022. Danvers: Vydavateľstvo IEEE, 2022, s. 211-214. ISBN 978-1-6654-6977-7.

[8] **SOBOTA, Michal** [20%]; NOVOTA, Miroslav [20%]; MIČJAN, Michal [20%]; HANIC, Michal [20%]; WEIS, Martin [20%]. Organic charge-modulated field-effect transistor for biosensing applications. ADEPT 2022. Žilina: Vydavateľstvo EDIS, 2022, s. 93-96. ISBN 978-80-554-1884-1.

[9] NOVOTA, Miroslav [31%]; **SOBOTA, Michal** [7%]; MIČJAN, Michal [31%]; WEIS, Martin [31%]. Organic pentacene and fullerene C60 inverters: The influence of gate dielectric. ASDAM 2020. Danvers: Vydavateľstvo IEEE, 2020, s. 51-54. ISBN 978-1-6654-6977-7.
Uložené v databáze: SCOPUS: 2-s2.0-85104535975

[10] KOKAVEC, Ondrej [5%]; NOVOTA, Miroslav [25%]; **SOBOTA, Michal** [20%]; MIČJAN [25%]; WEIS, Martin [25%]. Preparation technologies of OLED (organic light-emitting diodes) with emission dopant. ADEPT 2022. Žilina: Vydavateľstvo EDIS, 2022, s. 226-229. ISBN 978-80-554-1884-1.

[11] **SOBOTA, Michal** [5%]; NOVOTA, Miroslav [25%]; MIČJAN, Michal [25%]; PAVÚK, Milan [20%]; WEIS, Martin [25%]. Príprava a charakterizácia polymérnych dielektrík. 21. Škola vákuovej techniky. Bratislava: Slovenská vákuová spoločnosť, 2019, s. 149-153. ISBN 978-80-99905-01-7.

[12] **SOBOTA, Michal** [50%]; NOVOTA, Miroslav [5%]; REŽO, Vratislav [10%]; MIČJAN, Michal [15%]; Weis Martin [20%]. Real-time monitoring of PEDOT:PSS conductivity increase for organic electrochemical transistors. ADEPT 2023. Žilina: Vydavateľstvo EDIS, 2023, s. 230-233. ISBN 978-80-554-1977-0.

[13] NOVOTA, Miroslva [31%]; **SOBOTA, Michal** [7%]; MIČJAN, Michal [31%]; WEIS, Martin [31%]. ADEPT 2020. Žilina: Vydavateľstvo EDIS, 2020, s. 151-154. ISBN 978-80-554-1735-6

V3 Postery zo zahraničných konferencií (1)

[1] **SOBOTA, Michal** [40%]; VINCZE, Tomáš [10%]; REŽO, Vratislav [10%]; MIČJAN, Michal [15%]; TISOVSKÝ, Pavol [10%]; WEIS, Martin [15%]. Expanding the Application of OCMFETs: A pH Sensor and Novel Metal-Ion Detector. ICSM 2024. Dresden

Autor má 18 príspevkov z toho je 6 príspevkov v databáze SCOPUS.

10 Citačný ohlas uchádzača

FERIANCOVÁ, Lucia, et al. Dithienylnaphthalenes and quaterthiophenes substituted with electron-withdrawing groups as n-type organic semiconductors for organic field-effect transistors. Journal of Materials Chemistry C, 2022, 10.27: 10058-10074.

[1] AKIYAMA, Midori, et al. The Perfluoroadamantyl group: a bulky and highly electron-withdrawing substituent in thermally activated delayed fluorescence materials. Bulletin of the Chemical Society of Japan, 2024, 97.3: uoae025.

[2] ZHOU, Yang, et al. Molecular design concept for enhancement charge carrier mobility in OFETs: a review. Materials, 2023, 16.20: 6645.

[3] LI, Jianhui, et al. Design, synthesis, and application in OFET of a small molecule based on π-expanded fused diketopyrrolopyrrole. Frontiers in Chemistry, 2023, 11: 1280816.

EGYENES-PÖRSÖK, F., et al. Growth of α-and β-Ga2O3 epitaxial layers on sapphire substrates using liquid-injection MOCVD. Semiconductor Science and Technology, 2020, 35.11: 115002.

[1] WANG, Lixia, et al. Recent Progress in Solar-Blind Photodetectors Based on Ultrawide Bandgap Semiconductors. ACS omega, 2024, 9.24: 25429-25447.

[2] WOO, Kelly, et al. From wide to ultrawide-bandgap semiconductors for high power and high frequency electronic devices. Journal of Physics: Materials, 2024, 7.2: 022003.

[3] XIAO, Xinglin, et al. Phase-dependent phonon heat transport in nanoscale gallium oxide thin films. Small, 2024, 20.21: 2309961.

[4] HRUBIŠÁK, Fedor, et al. Heteroepitaxial growth of Ga2O3 on 4H-SiC by liquid-injection MOCVD for improved thermal management of Ga2O3 power devices. Journal of Vacuum Science & Technology A, 2023, 41.4.

[5] JEWEL, Mohi Uddin, et al. Phase Stabilized MOCVD Growth of β-Ga2O3 Using SiOx on c-Plane Sapphire and AlN/Sapphire Template. physica status solidi (a), 2023, 220.11: 2300036.

[6] LIU, Zeng; TANG, Weihua. A review of Ga2O3 deep-ultraviolet metal–semiconductor Schottky photodiodes. Journal of Physics D: Applied Physics, 2023, 56.9: 093002.
[7] Invited: Liquid-injection MOCVD-grown Ga2O3 on sapphire and 4H-SiC substrates: Material, transport, and MOSFET properties
[8] JEWEL, Mohi Uddin, et al. Demonstration of thick phase-pure β-Ga2O3 on a c-plane sapphire substrate using MOCVD. In: Oxide-based Materials and Devices XIV. SPIE, 2023. p. 18-22.
[9] BISWAS, Mahitosh; NISHINAKA, Hiroyuki. Thermodynamically metastable α-, ε-(or κ-), and γ-Ga2O3: From material growth to device applications. APL Materials, 2022, 10.6.
[10] YANG, Duyoung, et al. Epitaxial growth of alpha gallium oxide thin films on sapphire substrates for electronic and optoelectronic devices: Progress and perspective. Electronic Materials Letters, 2022, 18.2: 113-128.
[11] TAK, Bhera Ram, et al. Recent advances in the growth of gallium oxide thin films employing various growth techniques—a review. Journal of Physics D: Applied Physics, 2021, 54.45: 453002.
[12] ZHOU, Jingan, et al. Gallium oxide-based optical nonlinear effects and photonics devices. Journal of Materials Research, 2021, 1-14.
[13] HRUBIŠÁK, F., et al. Structural and electrical properties of Ga 2 O 3 transistors grown on 4H-SiC substrates. In: ASDAM 2022. IEEE, 2022. p. 115-118.

Sobota, M., et al. "Organic electrochemical transistors for biosensing applications." 2022 14th International Conference on Advanced Semiconductor Devices and Microsystems (ASDAM). IEEE, 2022.

[1] SHEN, Jiajun, et al. Anti-motion Interference Electrocardiograph Monitoring System-A Review. IEEE Sensors Journal, 2024.

Citácie: 17 citácií (z toho 17 citácií SCOPUS)

D1 Úžitkové vzory

Teplotný senzor na báze PEDOT:PSS, č. UV: 9559, zapísaný úžitkový vzor.

Organický poľom riadený tranzistor, č. UV: 9622, zapísaný úžitkový vzor.

11 Referecnes

1. TISOVSKÝ, Pavol, DONOVALOVÁ, Jana, KOŽÍŠEK, Jozef, HORVÁTH, Miroslav and GÁPLOVSKÝ, Anton. Reversible ON/OFF and OFF/ON, light-stimulated binding, or release processes of metal cations from isatin diarylhydrazone complexes in solution. Journal of Photochemistry and Photobiology A: Chemistry. 2022. Vol. 427, no. October 2021. DOI 10.1016/j.jphotochem.2022.113827.

2. TISOVSKÝ, Pavol, CSICSAI, Klaudia, DONOVALOVÁ, Jana, ŠANDRIK, Róbert, KOŽÍŠEK, Jozef and GÁPLOVSKÝ, Anton. Tautomerization of Z and E isomers of dipolar isatin bipyridylhydrazone complexes with Zn(II) ions. Photochromism - ON/OFF switching. Journal of Photochemistry and Photobiology A: Chemistry. 2021. Vol. 405, no. February 2020. DOI 10.1016/j.jphotochem.2020.112916.

3. LACE, Annija and CLEARY, John. A review of microfluidic detection strategies for heavy metals in water. Chemosensors. 2021. Vol. 9, no. 4. DOI 10.3390/chemosensors9040060.

4. WARNER, Kelly L., BARATAUD, Fabienne, HUNT, Randall J., BENOIT, Marc, ANGLADE, Juliette and BORCHARDT, Mark A. Interactions of Water Quality and Integrated Groundwater Management: Examples from the United States and Europe. In : Integrated Groundwater Management. Cham : Springer International Publishing, 2016. p. 347–376.

5. XI, Yue and XU, Pengfei. Global colorectal cancer burden in 2020 and projections to 2040. Translational Oncology. October 2021. Vol. 14, no. 10, p. 101174. DOI 10.1016/j.tranon.2021.101174.

6. FORREST, Stephen. Organic Electronics: Foundations to ApplicationsFoundations to Applications. 2020. ISBN 9780198529729.

7. KARUNAKARAN CHANDRAN, KALPANA BHARGAVA, Robson Bejamin. BIOSENSORS AND BIOELECTRONICS. 2015. ISBN 9780128031001.

8. KERGOAT, Loïg, PIRO, Benoît, BERGGREN, Magnus, HOROWITZ, Gilles and PHAM, Minh Chau. Advances in organic transistor-based biosensors: From organic electrochemical transistors to electrolyte-gated organic field-effect transistors. Analytical and Bioanalytical Chemistry. 2012. Vol. 402, no. 5, p. 1813–1826. DOI 10.1007/s00216-011-5363-y.

9. DEMELAS, Monia, LAI, Stefano, SPANU, Andrea, MARTINOIA, Sergio, COSSEDDU, Piero, BARBARO, Massimo and BONFIGLIO, Annalisa. Charge sensing by organic charge-modulated field effect transistors: Application to the detection of bio-related effects. Journal of Materials Chemistry B. 2013. Vol. 1, no. 31, p. 3811–3819. DOI 10.1039/c3tb20237b.

10. YASUDA, Akio and KNOLL, Wolfgang. Organic Bioelectronics for Life Science and Healthcare. 2019. ISBN 1644900378.

11. DEMELAS, Monia, LAI, Stefano, CASULA, Giulia, SCAVETTA, Erika, BARBARO, Massimo and BONFIGLIO, Annalisa. An organic, charge-modulated field effect transistor for DNA detection. Sensors and Actuators, B: Chemical. 2012. Vol. 171–172, p. 198–203. DOI 10.1016/j.snb.2012.03.007.

12. LAI, Stefano, VIOLA, Fabrizio Antonio, COSSEDDU, Piero and BONFIGLIO, Annalisa. Floating gate, organic field-effect transistor-based sensors towards biomedical applications fabricated with large-area processes over flexible substrates. Sensors (Switzerland). 2018. Vol. 18, no. 3, p. 1–12. DOI 10.3390/s18030688.

13. NAPOLI, Corrado, LAI, Stefano, GIANNETTI, Ambra, TOMBELLI, Sara, BALDINI, Francesco, BARBARO, Massimo and BONFIGLIO, Annalisa. Electronic detection of DNA hybridization by coupling organic field-effect transistor-based sensors and hairpin-shaped probes. Sensors (Switzerland). 2018. Vol. 18, no. 4. DOI 10.3390/s18040990.

14. SPANU, A., LAI, S., COSSEDDU, P., TEDESCO, M., MARTINOIA, S. and BONFIGLIO, A. An organic transistor-based system for reference-less electrophysiological monitoring of excitable cells. Scientific Reports. 2015. Vol. 5, p. 1–7. DOI 10.1038/srep08807.

15. SPANU, Andrea. The Micro Organic Charge Modulated FET Array. . 2016. P. 47–71. DOI 10.1007/978-3-319-28880-2_4.

16. WHITE, Scott P., DORFMAN, Kevin D. and FRISBIE, C. Daniel. Label-free DNA sensing platform with low-voltage electrolyte-gated transistors. Analytical Chemistry. 2015. Vol. 87, no. 3, p. 1861–1866. DOI 10.1021/ac503914x.

17. LAI, Stefano, BARBARO, Massimo and BONFIGLIO, Annalisa. Tailoring the sensing performances of an OFET-based biosensor. Sensors and Actuators, B: Chemical. 2016. Vol. 233, p. 314–319. DOI 10.1016/j.snb.2016.04.095.

18. LAI, S., DEMELAS, M., CASULA, G., COSSEDDU, P., BARBARO, M. and BONFIGLIO, A. Ultralow voltage, OTFT-based sensor for label-free DNA detection. Advanced Materials. 2013. Vol. 25, no. 1, p. 103–107. DOI 10.1002/adma.201202996.

19. MARTINEZ, J. and PIQUERAS, J. On the mobility of polycrystalline semiconductors. Solid-State Electronics [online]. April 1980. Vol. 23, no. 4, p. 297–303. DOI 10.1016/0038-1101(80)90196-3. Available from: https://linkinghub.elsevier.com/retrieve/pii/0038110180901963

20. MENICHELLI, M., BOSCARDIN, M., CRIVELLARI, M., DAVIS, J., DUNAND, S., FANÒ, L., MOROZZI, A., MOSCATELLI, F., MOVILEANU-IONICA, M., PASSERI, D., PETASECCA, M., PICCINI, M., ROSSI, A., SCORZONI, A., SERVOLI, L., VERZELLESI, G. and WYRSCH, N. Hydrogenated amorphous silicon detectors for particle detection, beam flux monitoring and dosimetry in high-dose radiation environment. Journal of Instrumentation [online]. 3 April 2020. Vol. 15, no. 04, p. C04005–C04005. DOI 10.1088/1748-0221/15/04/C04005. Available from: https://iopscience.iop.org/article/10.1088/1748-0221/15/04/C04005

21. MAGNANELLI, Timothy J. and HEILWEIL, Edwin J. Carrier mobility of silicon by sub-bandgap time-resolved terahertz spectroscopy. Optics Express [online]. 2 March 2020. Vol. 28, no. 5, p. 7221. DOI 10.1364/OE.382840. Available from: https://opg.optica.org/abstract.cfm?URI=oe-28-5-7221

22. INAL, Sahika, MALLIARAS, George G. and RIVNAY, Jonathan. Benchmarking organic mixed conductors for transistors. Nature communications. 24 November 2017. Vol. 8, no. 1, p. 1767. DOI 10.1038/s41467-017-01812-w.

23. TANG, Kan, MIAO, Wujian and GUO, Song. Crosslinked PEDOT:PSS Organic Electrochemical Transistors on Interdigitated Electrodes with Improved Stability. ACS Applied Polymer Materials. 12 March 2021. Vol. 3, no. 3, p. 1436–1444. DOI 10.1021/acsapm.0c01292.

24. OSAZUWA, Peter O., LO, Chun-Yuan, FENG, Xu, NOLIN, Abigail, DHONG, Charles and KAYSER, Laure V. Surface Functionalization with (3-Glycidyloxypropyl)trimethoxysilane (GOPS) as an Alternative to Blending for Enhancing the Aqueous Stability and Electronic Performance of PEDOT:PSS Thin Films. ACS Applied Materials &

Interfaces. 29 November 2023. Vol. 15, no. 47, p. 54711–54720. DOI 10.1021/acsami.3c09452.

25. ZHANG, Shiming, KUMAR, Prajwal, NOUAS, Amel Sarah, FONTAINE, Laurie, TANG, Hao and CICOIRA, Fabio. Solvent-induced changes in PEDOT:PSS films for organic electrochemical transistors. APL Materials. 1 January 2015. Vol. 3, no. 1. DOI 10.1063/1.4905154.

26. MASSETTI, Matteo, ZHANG, Silan, HARIKESH, Padinhare Cholakkal, BURTSCHER, Bernhard, DIACCI, Chiara, SIMON, Daniel T., LIU, Xianjie, FAHLMAN, Mats, TU, Deyu, BERGGREN, Magnus and FABIANO, Simone. Fully 3D-printed organic electrochemical transistors. npj Flexible Electronics. 7 March 2023. Vol. 7, no. 1, p. 11. DOI 10.1038/s41528-023-00245-4.

27. AARIK, Lauri, PILLER, Carl Thomas, RAUD, Jüri, TALVISTE, Rasmus, JÕGI, Indrek and AARIK, Jaan. Atomic layer deposition of α-Al2O3 from trimethylaluminum and H2O: Effect of process parameters and plasma excitation on structure development. Journal of Crystal Growth. 2023. Vol. 609, no. January, p. 6–11. DOI 10.1016/j.jcrysgro.2023.127148.

28. CHEN, Yanyan, DENG, Wei, ZHANG, Xiujuan, WANG, Mingxiang and JIE, Jiansheng. Ambient instability of organic field-effect transistors and their improvement strategies. Journal of Physics D: Applied Physics [online]. 3 February 2022. Vol. 55, no. 5, p. 053001. DOI 10.1088/1361-6463/ac2ad3. Available from: https://iopscience.iop.org/article/10.1088/1361-6463/ac2ad3

29. SHIH, Ching-Chieh, LEE, Yeong-Shyang, FANG, Kuo-Lung, CHEN, Ching-Hung and GAN, Feng-Yuan. A Current Estimation Method for Bias-Temperature Stress of a-Si TFT Device. IEEE Transactions on Device and Materials Reliability [online]. June 2007. Vol. 7, no. 2, p. 347–350. DOI 10.1109/TDMR.2007.901068. Available from: http://ieeexplore.ieee.org/document/4295101/

30. SHIN, Hyeonwoo, ROH, Jeongkyun, SONG, Jiyoung, ROH, Heebum, KANG, Chan-Mo, LEE, Taesoo, PARK, Gunbaek, AN, Kunsik, KIM, Jun Young, KIM, Hyoseok, KWAK, Jeonghun, LEE, Changhee and KIM, Hyeok. Highly Stable Organic Transistors on Paper Enabled by a Simple and Universal Surface Planarization Method. Advanced Materials Interfaces [online]. 6 April 2019. Vol. 6, no. 8. DOI 10.1002/admi.201801731. Available from: https://onlinelibrary.wiley.com/doi/10.1002/admi.201801731

31. LEE, Hansol, MOON, Byungho, SON, Sung Yun, PARK, Taiho, KANG, Boseok and CHO, Kilwon. Charge Trapping in a Low-Crystalline High-Mobility Conjugated Polymer and Its Effects on the Operational Stability of Organic Field-Effect Transistors. ACS Applied Materials & Interfaces [online]. 14 April 2021. Vol. 13, no. 14, p. 16722–16731. DOI 10.1021/acsami.0c20965. Available from: https://pubs.acs.org/doi/10.1021/acsami.0c20965

32. RASHID, Jahwarhar Izuan Abdul and YUSOF, Nor Azah. The strategies of DNA immobilization and hybridization detection mechanism in the construction of electrochemical DNA sensor: A review. Sensing and Bio-Sensing Research [online]. 2017. Vol. 16, no. October, p. 19–31. DOI 10.1016/j.sbsr.2017.09.001. Available from: http://dx.doi.org/10.1016/j.sbsr.2017.09.001